

Research Paper

Gold Clusters Prevent Inflammation-Induced Bone Erosion through Inhibiting the Activation of NF- κ B Pathway

Qing Yuan¹, Fuping Gao², Yawen Yao¹, Pengju Cai², Xiangchun Zhang², Jinling Yuan¹, Kaixiao Hou¹, Liang Gao¹, Xiaojun Ren¹, Xueyun Gao^{1,2}✉

1. Department of Chemistry and Chemical Engineering, Beijing University of Technology, Beijing 100124, China

2. CAS Key Laboratory for the Biological Effects of Nanomaterials and Nanosafety, Institute of High Energy Physics, Chinese Academy of Sciences, Beijing 100049, China

✉ Corresponding author: Department of Chemistry and Chemical Engineering, Beijing University of Technology, Beijing 100124, China. E-mail address: gaoyx@ihp.ac.cn (X. Gao)

© Ivyspring International Publisher. This is an open access article distributed under the terms of the Creative Commons Attribution (CC BY-NC) license (<https://creativecommons.org/licenses/by-nc/4.0/>). See <http://ivyspring.com/terms> for full terms and conditions.

Received: 2018.11.29; Accepted: 2019.01.28; Published: 2019.03.01

Abstract

Inflammation-induced bone erosion is a major pathological factor in several chronic inflammatory diseases that often cause severe outcomes, such as rheumatoid arthritis and periodontitis. Plenty of evidences indicated that the inflammatory bone destruction was attributed to an increase in the number of bone-resorbing osteoclasts. However, anti-resorptive therapy alone failed to prevent bone loss in an inflammatory condition. Conventional anti-inflammation treatments are usually intended to suppress inflammation only, but ignore debilitating the subsequent bone destruction. Therefore, inhibition of proinflammatory activation of osteoclastogenesis could be an important strategy for the development of drugs aimed at preventing inflammatory bone destruction.

Methods: In this study, we synthesized a peptide coated gold cluster to evaluate its effects on inflammatory osteoclastogenesis *in vitro* and inflammation-induced bone destruction *in vivo*. The *in vitro* anti-inflammation and anti-osteoclastogenesis effects of the cluster were evaluated in LPS-stimulated and receptor activator of nuclear factor κ B ligand (RANKL) stimulated macrophages, respectively. The LPS-induced expression of crucial pro-inflammation cytokines and RANKL-induced osteoclastogenesis as well as the activation of NF- κ B pathway in both situations were detected. The inflammation-induced RANKL expression and subsequent inflammatory bone destruction *in vivo* were determined in collagen-immunized mice.

Results: The gold cluster strongly suppresses RANKL-induced osteoclast formation *via* inhibiting the activation of NF- κ B pathway *in vitro*. Moreover, treatment with the clusters at a dose of 5 mg Au/kg.bw significantly reduces the severity of inflammation-induced bone and cartilage destruction *in vivo* without any significant toxicity effects.

Conclusion: Therefore, the gold clusters may offer a novel potent therapeutic stratagem for inhibiting chronic inflammation associated bone destruction.

Key words: gold cluster, osteoclastogenesis, inflammatory bone destruction, NF- κ B pathway

Introduction

Inflammation-induced progressive bone destruction is a major pathological feature of chronic inflammatory diseases, including rheumatoid arthritis (RA), periodontitis and osteoporosis [1-3]. Conventional treatments for such chronic inflammatory

diseases are intended to inhibit inflammation only, but few treatments are debilitating of inflammatory bone destruction [4, 5]. However, even under anti-inflammation treatment, a large number of patients continue to suffer from such severe bone

destruction [1, 6]. Therefore, there is an urgent need for more effective therapeutics to reduce inflammation-induced bone destruction.

Bone erosion is considered to be mediated primarily by enhanced activation of osteoclasts (OCs) [6, 7]. In the pathogenesis of chronic inflammatory diseases, focal bone erosion is also predominantly generated by an increase in the number of bone-resorbing osteoclasts [4, 8]. The most crucial cytokine involved in osteoclast development and activation is the receptor activator of nuclear factor κ B ligand (RANKL), which belongs to the TNF family [7]. Expression of RANKL may be regulated by several pro-inflammatory cytokines, including tumor necrosis factor (TNF- α), interleukin 1 (IL-1) and interleukin 6 (IL-6) [7, 9]. Therefore, inhibition of pro-inflammatory activation of osteoclastogenesis could be an important strategy for the development of drugs aimed at preventing inflammatory bone destruction.

Recent years, gold clusters have attracted more attention for their excellent biocompatibilities and synergistic biomedical properties [10, 11]. In this study, we firstly synthesized a peptide coated gold cluster to evaluate its effects on inflammatory osteoclastogenesis *in vitro* and inflammation-induced bone destruction *in vivo*. The results showed that the gold cluster can significantly inhibit inflammation-induced RANKL expression and subsequent RANKL-triggered osteoclast differentiation, blocking inflammatory bone destruction in collagen-immunized DBA/1 mice without any significant toxicity effects. Further studies suggest that disruption of the activation of NF- κ B pathway may contribute to osteoclastogenesis inhibition and bone protection activities of the gold cluster.

Methods

Reagents and cell line

All chemical reagents were purchased from Sigma-Aldrich (USA). The peptides were purchased from China Peptides Co. Ltd. (purity: 95%). All the primary antibodies were purchased from Cell Signaling Technology Inc., (USA) and the secondary antibody was bought from Beyotime Biotechnology (China). The blocking buffer and primary antibody dilution buffer for western blot were obtained from Beyotime Biotechnology. All cell culture reagents were purchased from Thermo Fisher Scientific Inc. (Gibco™, USA). The mouse macrophage RAW 264.7 cell was obtained from the American Type Culture Collection (ATCC). Recombinant Mouse RANKL was purchased from R&D systems, Inc. (USA).

Preparation of Au₂₅Sv₉ clusters

An aqueous solution of HAuCl₄ (25 mM, 16 μ L)

was slowly added to peptide solution (1.06 mM, 376 μ L) in a 5 mL vial under vigorous stirring, and then NaOH (0.5 M, 8 μ L) was added within 30 s to give a final pH of 10. The sample was sealed and stored in darkness for 15 h avoiding any disturbance to produce the Au₂₅peptide₉ products. The as-synthesized products were dialyzed for 12 h (Dialysis Tube MWCO: 500) to remove free HAuCl₄ and NaOH. Then the sample was further concentrated by using an ultrafiltration tube (Millipore, USA, MWCO3000) to remove free peptides. The purified Au₂₅peptide₉ was sterilized by filtration with 0.22 μ m filter for cell treatment. An aliquot was detected by ICP-MS to quantify the Au content and the rest was sealed and stored in dark under 4 °C.

Characterization of Au₂₅Sv₉ clusters

A PerkinElmer (LS-55) fluorescence spectrometer (PerkinElmer, USA) with Xe lamp was used to detect the excitation/emission spectra of Au₂₅Sv₉. The excitation and emission slits were both 10 nm and the scanning speed was 400 nm/min. The synthetic Au₂₅Sv₉ was observed by high-resolution transmission electron microscopy (HRTEM). Samples were prepared by casting and evaporating on a 300-mesh holey carbon-coated copper grid (Electron Microscopy Sciences, Washington, USA). High resolution images were obtained by TENCAI F20 high resolution transmission electron microscopy (FEI, USA) at 200 kV accelerating voltage. The molecular composition of the synthesized clusters was analyzed by matrix-assisted laser desorption/ionization time of flight mass spectrometry (MALDI-TOF MS). An ABI MALDI-TOF system in positive ion linear mode was used. The α -Cyano-4-hydroxycinnamic acid was used as the matrix. Detections were repeated for three times.

Cell viability assay

The viability of RAW264.7 cells was measured by using Cell Counting Kit (CCK-8) (Dojindo Laboratories, Japan). Cells were seeded into 96-well plates at the density of 1×10^4 cells/well in triplicate. After incubation for 24 h, fresh medium containing different dose of Au₂₅Sv₉ was added and incubated for another 48 h. At the indicated time, 1/10 (v/v) CCK-8 solution was added to each well and incubated for 1 h at 37 °C. The absorbency at 450 nm of each wells were measured by a 96-well plate reader (MD, USA).

Osteoclastogenic culture of RAW264.7 cells

For osteoclastogenesis induction, RAW264.7 cells were seeded into 48-well plates at the density of 1×10^4 cells/well and incubated in complete DMEM medium containing 50 ng/mL RANKL (R&D

Systems) for indicated days to generate osteoclasts. The inducing medium was refreshed every two days.

Tartrate-resistant acid phosphatase (TRAP) staining assay

After osteoclastogenic inducing for 6 days in the presence of different dose of Au₂₅Sv₉ (0.4, 2 and 4 μM), the RAW264.7 cells were washed with PBS twice and fixed with 3.7% paraformaldehyde for 15 min at room temperature followed by permeabilization with 0.1% triton X-100 for 10 min. Fixed cells were stained by using tartrate-resistant acid phosphatase (TRAP) staining kit (387A-1KT, Sigma-Aldrich) for 1 h at 37 °C in the dark following the manufacturer's instructions. TRAP-positive multinucleated (nuclei > 3) cells were counted as osteoclasts using a light microscope (IX71; Olympus).

Actin ring formation assay

RAW264.7 cells were seeded in confocal dishes at the density of 2 × 10⁴ cells/dish and incubated in inducing medium for 6 days in the presence of different dose of Au₂₅Sv₉ (0.4, 2 and 4 μM) to form actin rings. Then, the cells were washed twice with PBS and fixed with 3.7% paraformaldehyde for 20 min followed by permeabilization with 0.1% triton X-100 for 15 min at room temperature. Actin rings were stained by rhodamine-conjugated phalloidin (Cytoskeleton, Inc., Denver, USA) after washed with PBS, and cell nucleus were stained with DAPI (Sigma-Aldrich) for 5 min. The formation of actin rings in each sample was visualized by confocal laser scanning microscopy (Nikon Ti-E imaging system, Tokyo, Japan).

Bone resorption assay

RAW264.7 cells were cultured in Corning Osteo Assay Surface 24-well plates coated with calcium phosphate substrate at the density of 2 × 10⁴ cells/well. The medium was removed after 24 h incubation and inducing medium containing different dose of Au₂₅Sv₉ (0.4, 2 and 4 μM) was added. Culture medium was refreshed every two days. After about 6 days, cells were removed with a 10% sodium hypochlorite and rinsed for three times with water. The bone resorption pits were observed and photographed by light microscope. Image J software was used to quantify the percentage of resorbed bone surface area.

Quantitative real-time polymerase chain reaction (RT-PCR)

RAW264.7 cells were incubated with complete DMEM medium containing 50 ng/mL RANKL and different dose of Au₂₅Sv₉ (0.4, 2 and 4 μM) for 48 h. Total RNA was prepared by using an RNeasy Plus

Mini Kit (Qiagen, Hilden, NW, Germany), and reverse transcribed with Oligo (dT)₁₅ primer and M-MLV reverse transcriptase following the manufacturer's instructions (Promega, Fitchburg, WI, USA). The transcription of osteoclasts related genes were evaluated, including NFATc1, c-Fos, TRAP, and OSCAR. Quantitative RT reactions were performed by using iQTM SYBR[®] Green Supermix and iQTM5 Multicolor Real-Time PCR Detection System (Bio-Rad Laboratories, Inc., Hercules, CA, USA) according to the manufacturer's recommendations. GAPDH was used as the internal control and the primers were as follows: NFATc1, forward 5'-TGT TCT TCC TCC CGA TGT CT-3' and reverse 5'-CCC GTT GCT TCC AGA AAA TA-3'; c-Fos, forward 5'-TTG CTG ATG CTC TTG ACT GG-3' and reverse 5'-GGA TTT GAC TGG AGG TCT GC-3'; TRAP, forward 5'-CTG GAG TGC ACG ATG CCA GCG ACA-3 and reverse 5'-TCC GTG CTC GGC GAT GGA CCA GA-3'; OSCAR, forward 5'-CTG CTG GTA ACG GAT CAG CTC CCC AGA-3' and reverse 5'-CCA AGG AGC CAG AAC CTT CGA AAC T-3'; GAPDH, forward 5'-AAA TGG TGA AGG TCG GTG TG-3' and reverse 5'-TGA AGG GGT CGT TGA TGG-3'.

Western blotting

Cells were lysed in ice-cold RIPA lysis buffer (Beyotime, China) containing protease inhibitors (Roch), incubated on ice for 20 min, and centrifuged at 4 °C at 12,000 g. For endonuclear protein detection, cytoplasmic and nuclear proteins were extracted separately by using the Nuclear and Cytoplasmic Protein Extraction Kit (Beyotime Biotechnology). The supernatants were collected from each sample and protein concentrations were determined by the BCA reagent (Beyotime, China). Protein samples were mixed with SDS-PAGE loading buffer (Beyotime, China) and then heated at 95 °C for 5 min. Samples were subsequently resolved on 12% Bis-Tris acrylamide gels, and transferred to PVDF membrane. After blocking with block buffer, the membranes were incubated with specific primary antibodies against IκBα, p-IκBα, NF-κB, p-NF-κB, ERK, p-ERK, JNK, p-JNK, p38, p-p38, Akt and p-Akt (Cell Signaling Technology, Danvers, MA) overnight at 4 °C. After being rinsed three times, the membranes were incubated with corresponding secondary antibodies (Cell Signaling Technology, Danvers, MA) for 1 h at room temperature. Immunoreactive bands were visualized by using the enhanced chemiluminescence (ECL) reagent (GE). For densitometric analysis, ImageJ software (the National Institutes of Health, USA) was used.

Reverse transcription-polymerase chain reaction (RT-PCR)

RAW264.7 cells were incubated with complete DMEM medium containing 1 µg/mL LPS and different dose of Au₂₅Sv₉ (0.4, 2 and 4 µM) for 48 h. Total RNA was prepared by using an RNeasy Plus Mini Kit (Qiagen, Hilden, NW, Germany), and reverse transcribed with Oligo (dT)₁₅ primer and M-MLV reverse transcriptase following the manufacturer's instructions (Promega, Fitchburg, WI, USA). The transcription of pro-inflammatory factors was evaluated, including TNF-α, IL-1β and IL-6. PCR reactions were performed by using Q5® High-Fidelity PCR Kit (New England Biolabs, Inc., USA) according to the manufacturer's recommendations. The β-actin was used as an internal control. The amplification products were visualized by agarose gel electrophoresis. The primers were as follows: IL-1β, forward 5'-CAG GAT GAG GAC ATG AGC ACC-3', and reverse 5'-CTC TGC AGA CTC AAA CTC CAC-3'; TNF-α, forward 5'-CCT GTA GCC CAC GTC GTA GC-3', and reverse 5'-TTG ACC TCA GCG CTG AGT TG-3'; IL-6, forward 5'-GTA CTC CAG AAG ACC AGA GG-3', and reverse 5'-TGC TGG TGA CAA CCA CGG CC-3'; and β-actin, forward 5'-GTG GGC CGC CCT AGG CAC CAG-3', and reverse 5'-GGA GGA AGA GGA TGC GGC AGT-3'.

Collagen-induced arthritis (CIA) model and assessment

All animal care and experiments were approved by the Institutional Animal Care and Ethic Committee at the Chinese Academy of Sciences (Approved No. SYXK(jing)2014-0023). Native bovine type II collagen (Chondrex, Inc.) was dissolved in 0.1 mM acetic acid at 4 °C overnight and then emulsified with an equal volume of Complete Freund's Adjuvant (Chondrex, Inc) to prepare a 1 mg/mL immune emulsion. Male 6-week-old DBA/1 mice (Beijing Huafukang bioscience Co., Inc.) were subcutaneously (s.c.) injected at the base of the tail with 0.1 mL of emulsion containing 100 µg of type II collagen. At day 21 after the primary immunization, mice were boosted (s.c.) with 100 µg type II collagen immune emulsion once again. The day after the secondary immunization, mice were treated with Au₂₅Sv₉ or saline. The gold clusters were administered i.p. daily at dose of 5 mg Au/kg/day until day 49 after primary immunization. Mice were closely monitored for arthritis disease progression every second day and detected two clinical parameters: ankle circumference and clinical arthritis score. Each limb was graded, and a mean score was calculated for each animal. Body weight of each mouse was also measured every week. At day 49 after primary immunization, blood was collected

from each mice for haematological and blood biochemical analysis. The hind limb of each mouse was harvested after sacrificed and imaged with three-dimensional microfocus computed tomography (IVIS Spectrum CT, Perkin Elmer, USA). For histological analysis, hind paws of 5 mice in each group were randomly collected and fixed with 10% paraformaldehyde, then decalcified in 10% EDTA and embedded in paraffin. 5-µm microsection slices were stained with haematoxylin and eosin or indicated antibody. The levels of phosphorylated NF-κB in the histologic sections were quantized by using Color Detection module of Immunohistochemistry (IHC) Image Analysis Toolbox in Image J software, according to the manufacturer's instructions [12]. Joint samples of other 5 mice in each group were isolated from the hind paws and homogenized by ultra-low temperature grinding. The concentrations of TNF-α, IL-1β and IL-6 in the joint tissues lysate were determined using corresponding ELISA kits (Shanghai jianglaibio Co., LTD, China) according to the manufacturer's instructions. Measurement of RANKL was performed on the same samples using Western immunoblotting. The major organs were also excised and fixed in 10% formalin for histopathological examination.

Statistical analysis

Statistical analysis was performed using SPSS ver. 19.0 software (SPSS, Chicago, IL). Data are represented as mean ± Standard deviation (SD). Statistical differences were assessed by a one-way ANOVA and P < 0.05 was considered to be significant.

Results

Preparation and characterization of Au₂₅Sv₉ gold cluster

The gold clusters were synthesized and purified according to a mature method we have established [13, 14]. Briefly, Sv peptide was used to anchor Au cluster via strong Au-S bonds in aqueous solution under mild conditions. Au₂₅Sv₉ has excellent water-solubility and the solution displays a clear red-brown colour under sunlight and emits a strong red fluorescence under UV light excited (Figure 1A). Spectral analysis showed the peaks of excitation and emission spectra at 560 nm (red curve) and 656 nm (black curve), respectively (Figure 1B). The precise molecular formula of the cluster was identified by matrix-assisted laser desorption/ionization time of flight mass spectrometry (MALDI-TOF MS) in positive ion mode. The mass spectra consisted of serial strong peaks between 5k-20k m/z and the step between adjacent intense peaks matched with

the m/z of one peptide cut two thiol groups (Figure 1C). According to previous reports, Au_{25} cluster should be stabilized by 18 -SH groups, and each Sv peptide has two Cys. Therefore, we can speculate that the Au_{25} cluster is coated with 9 peptides [15, 16]. This assumption is confirmed by the serial intense peak in Figure 1C, where the first m/z peak matches the $Au_{25}S_{18}$ formula.

Effects of $Au_{25}Sv_9$ on LPS-induced inflammation *in vitro*

Several pro-inflammatory cytokines have been proved to be crucial in regulating the onset and progression of inflammatory bone destruction in chronic inflammatory diseases, including TNF- α , IL-1 and IL-6 [1, 17, 18]. Therefore, we investigated the anti-inflammation activity of $Au_{25}Sv_9$ in LPS-stimulated RAW264.7 cells. The cell viability of RAW264.7 cells with different concentrations of $Au_{25}Sv_9$ was firstly determined by CCK-8 assay. It was found that $Au_{25}Sv_9$ did not induce any significant cytotoxic effect on RAW264.7 cells even at concentrations up to 20 μ M after 48 hour of incubation (Figure 2A). Immunoblotting detection showed that the secretions of TNF- α , IL-1 β and IL-6 were all increased by LPS stimulation, and was suppressed by adding $Au_{25}Sv_9$ in a dose-dependent manner (Figure 2B). The transcriptional regulation of these cytokines was further determined by RT-PCR assay. The results indicated the transcriptional inhibitory activity of $Au_{25}Sv_9$ on LPS-induced overexpression of these pro-inflammatory cytokines (Figure 2C). There are conclusive evidences that the transcription factor NF- κ B is critical for transcription of these cytokines in chronic inflammation diseases [19, 20]. Therefore, activation of the NF- κ B pathway in LPS-stimulated RAW264.7 cells in the presence or absence of $Au_{25}Sv_9$ was detected by immunoblotting. According to the results, the phosphorylation of I κ B and nuclear translocation of NF- κ B were significantly enhanced by LPS when compared to the mock treatment. Supplementation of $Au_{25}Sv_9$ significantly inhibited the activation of NF- κ B in a dose-dependent manner (Figure 2D). In addition, the inhibitory effects of the clusters on the LPS-induced activation of NF- κ B as well as the secretion of IL-1 β and IL-6 were also proved in bone marrow-derived macrophages (BMDMs) (Figure S1). These results indicated that the gold cluster possesses an anti-inflammation potent in activated macrophage.

Effects of $Au_{25}Sv_9$ on RANKL-induced osteoclast formation and bone resorption *in vitro*

Inflammation-induced bone erosion is caused by

an increase in the number of bone-resorbing osteoclasts mediated by RANKL stimulation [5, 9, 21]. RANKL directly regulates the differentiation of osteoclast (OC) from monocyte/macrophage precursor cells and increases their expression by aforesaid pro-inflammatory cytokines under chronic inflammatory conditions [7, 9]. We next evaluated the effect of $Au_{25}Sv_9$ on RANKL-induced osteoclastogenesis *in vitro*. OCs differentiation from RAW264.7 cells could be identified by tartrate-resistant acid phosphatase (TRAP) staining [22, 23]. Therefore, the number of TRAP+ multinucleated cells (TRAP+ MNCs) in each treatment was counted. As shown in Figure 3A, on day 6 of culture, 50 ng/mL RANKL successfully induced osteoclastogenesis in both presence and absence of $Au_{25}Sv_9$. It was visually observed that RANKL alone induced the highest number of TRAP+ MNCs and supplementation of $Au_{25}Sv_9$ significantly decreased the amount in a dose-dependent manner (Figure 3A). $Au_{25}Sv_9$ inhibited the formation of TRAP+ MNCs from 100% (control) to 69.6%, 41.1%, and 14.3% at 0.4, 2, and 4 μ M, respectively (Figure 3B). It's worth noting that, the Sv peptide alone did not affect the formation of TRAP+ MNCs induced by RANKL at an equal dose of 4 μ M $Au_{25}Sv_9$, excluding the effect of peptides on osteoclastogenesis. Considering that $Au_{25}Sv_9$ did not have any significant effect on the viability of RAW 264.7 cells at selected concentrations (Figure 2A), it was demonstrated that the inhibitory effect of $Au_{25}Sv_9$ on osteoclast formation was not caused by cytotoxicity.

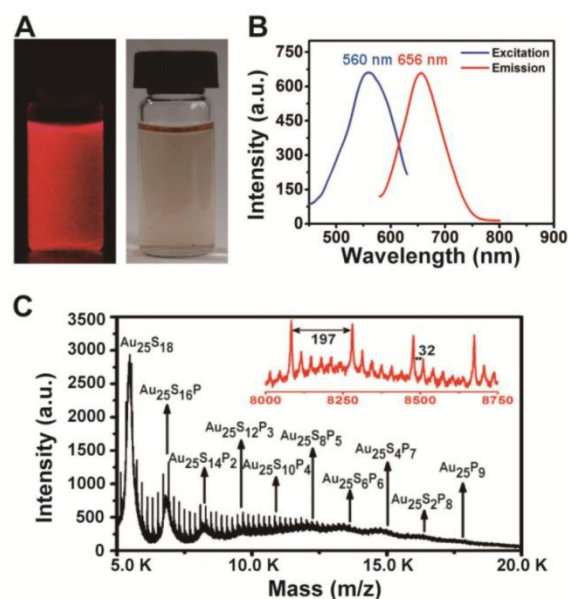


Figure 1. Characterization of the synthesized $Au_{25}Sv_9$ cluster. (A) The photographs of the $Au_{25}Sv_9$ solution under visible light and UV light. (B) The fluorescence excitation and emission spectra of $Au_{25}Sv_9$ (650 nm and 551 nm). (C) The MALDI-TOF-MS spectra of $Au_{25}Sv_9$, which can be expressed by formula of $Au_{25}Sv_n$. The insets showed weak peaks from m/z 8.0 k to 8.75 k, the m/z 197 and 32 correspond to the single Au and S, respectively.

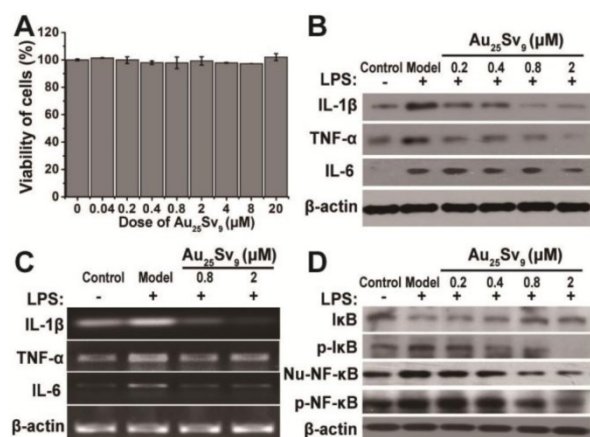


Figure 2. Effects of Au₂₅Sv₉ on LPS-induced expression of inflammatory cytokines and signaling pathways. (A) Cell viability of RAW264.7 in the presence of different dose of Au₂₅Sv₉ was measured using the CCK-8 assay, the data is presented as mean ± Standard deviation of triplicate experiments. (B) Western blotting for secretion of TNF-α, IL-1β and IL-6 in LPS-stimulated RAW264.7 cells in the presence or absence of Au₂₅Sv₉. (C) Transcriptional regulation of these cytokines by Au₂₅Sv₉ was determined by RT-PCR assay, β-actin was used as the loading control. (D) The LPS-induced activation of NF-κB in the presence or absence of Au₂₅Sv₉ was detected by Western blotting (degradation of IκB and nuclear translocation of NF-κB), β-actin was used as the loading control. Nu-NF-κB indicated as nuclei-NF-κB. Data was from three independent experiments and one representative result is shown here.

The formation of large multinuclear cells after pre-osteoclast fusion is critical for osteoclast-mediated bone resorption [6]. The fused large multinuclear cells will display an actin ring that allows them to resorb bone [24, 25]. Therefore, the actin ring formation of RAW264.7 cells induced by RANKL with or without Au₂₅Sv₉ was detected by immunofluorescence staining. RANKL was found to be effective in stimulating actin ring formation, while Au₂₅Sv₉ reduced it in a dose-dependent manner (Figure 3C). Supplementation of 4 μM Au₂₅Sv₉ showed almost no actin ring formation. This unique cytoskeletal structure allows osteoclasts to seal a zone on the bone surface and increase the activity of proteases on bone-resorption [25]. Thus, the effect of Au₂₅Sv₉ on the bone resorption activity of OCs formed *in vitro* was assessed by a pit formation assay on the surface of osteoassay plate (Figure 3D). Quantitative analysis of the ratio of resorption pits per unit area of the osteoassay plate indicated that Au₂₅Sv₉ reduced RANKL induced resorption pits formation in a dose-dependent manner (Figure 3E). Based on these results, we deduced that the gold cluster can block the formation of multinucleated OCs and reduce their bone resorption activity *in vitro*.

Effects of Au₂₅Sv₉ on the expression of osteoclastogenic genes and RANKL-induced signaling pathways

The processes of differentiation, maturation and function of OCs are directly regulated by osteoclastogenic genes [6]. To investigate the effect of Au₂₅Sv₉ on

the expression of OC-specific genes in RANKL-treated RAW264.7 cells, real-time PCR was used to determine mRNA expression. Cells treated with or without RANKL were used as positive and negative controls, respectively, and GAPDH was used as an internal reference to normalize each group. NFATc1 and c-Fos are two pivotal OC-specific transcription factors involved in OC differentiation and are up-regulated following RANKL stimulation. As shown in Figure 4A, stimulation of RAW264.7 cells with RANKL induced over-expressions of both c-Fos and NFATc1, whereas supplementation of Au₂₅Sv₉ significantly decreased expression levels in a dose-dependent manner. The mRNA expressions of TRAP and OSCAR, two OC-specific genes that enhanced by c-Fos and NFATc1, were also significantly inhibited by supplementation of Au₂₅Sv₉ (Figure 4B). This expression regulation of TRAP correlated well with prior TRAP+ MNCs generation results (Figure 3A). Overall, Au₂₅Sv₉ significantly down-regulate the over-expression of RANKL-induced osteoclastogenic genes.

Under inflammatory conditions, higher level of RANKL will trigger a variety of intracellular signal transduction events leading to up-regulation of osteoclast-specific genes [7]. Gene targeting studies indicate that NF-κB and mitogen-activated protein kinases (MAPKs) are the paramount downstream signaling pathways of RANKL stimulation that have crucial role in osteoclast differentiation [6, 7]. To investigate the biological mechanisms of inhibitory effects of Au₂₅Sv₉ on RANKL-induced OC differentiation, these signaling pathways were detected by Western blotting (Figure 4C-D). RAW264.7 cells were stimulated with RANKL in the presence or absence of Au₂₅Sv₉ and the activation of MAPKs (p38, ERK, and JNK) and NF-κB were measured at predetermined time points. RANKL stimulation significantly enhanced the phosphorylation of IκB and NF-κB compared to the absence of RANKL treatment (Figure 4C). Supplementation of Au₂₅Sv₉ significantly inhibited the activation of NF-κB in a dose-dependent manner (Figure 4C). Phosphorylated proteins are active forms of MAPKs that are increased by RANKL stimulation, but supplementation of Au₂₅Sv₉ did not significantly suppress their activation at selected time points (Figure 4D). These results indicated that RANKL-induced activation of NF-κB signaling pathway was specifically down-regulated by Au₂₅Sv₉. In addition, we detected the activation of another RANKL-induced signal pathway, AKT, which is important for inhibition of OC cell death. Phosphorylation levels of AKT were increased by RANKL stimulation, but decreased in the presence of Au₂₅Sv₉ (Figure 4C). This indicated that the AKT signaling pathway is also down-regulated by Au₂₅Sv₉.

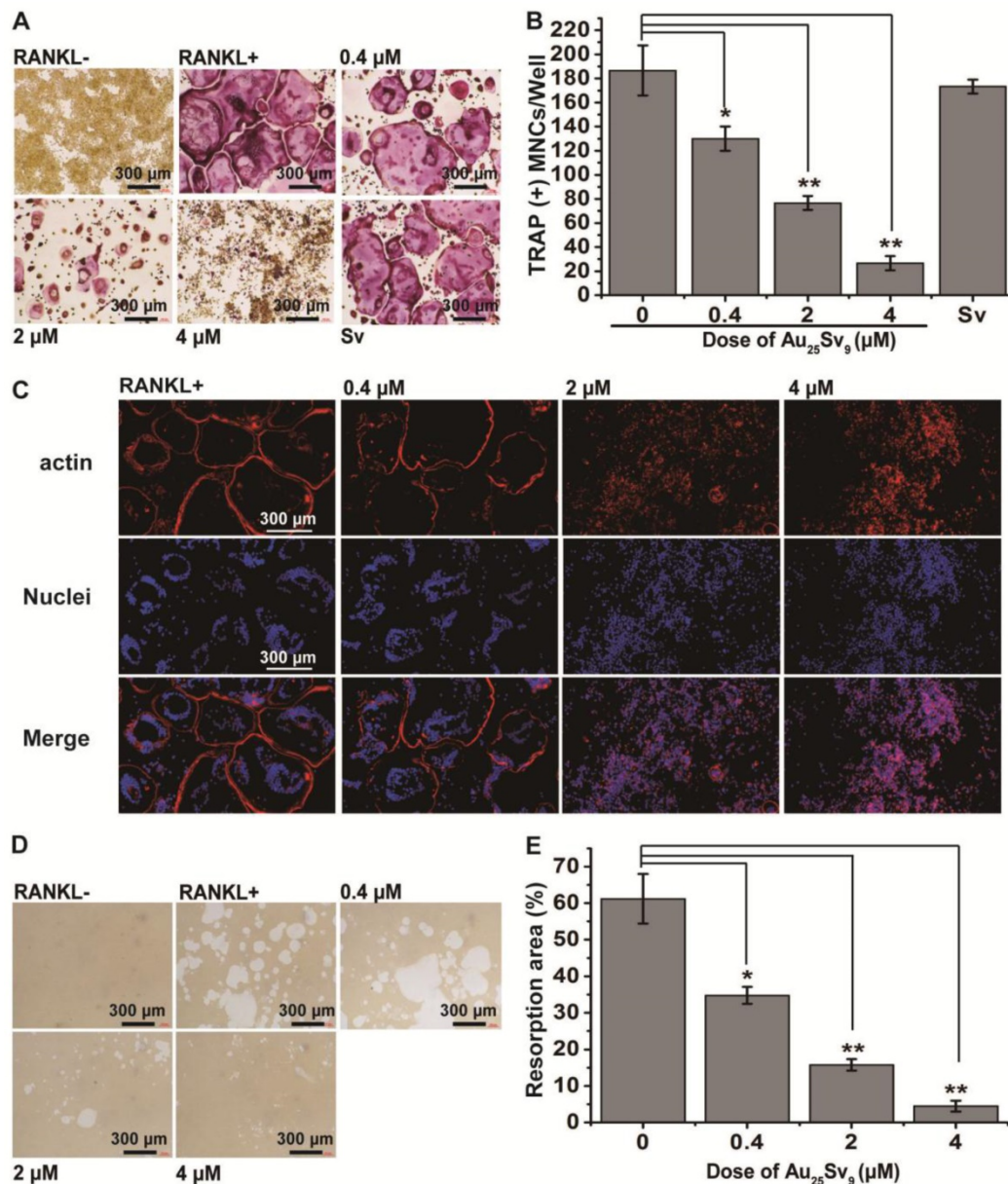


Figure 3. Effects of Au₂₅Sv₉ on RANKL-induced osteoclast formation and bone resorption *in vitro*. (A) RANKL stimulated RAW264.7 cells were treated with or without the indicated dose of Au₂₅Sv₉ and were stained with TRAP staining. Sv group indicated the equal dose of Sv peptide as 4 μM Au₂₅Sv₉. Data was from three independent experiments and one representative result is shown here. (B) The number of TRAP+ multinucleated cells (TRAP+ MNCs) in each treatment was counted. The data is presented as mean ± Standard deviation of triplicate experiments, *P < 0.05, **P < 0.01, compared to the RANKL only group. (C) The actin-ring formation of RAW264.7 cells induced by RANKL with or without Au₂₅Sv₉ was detected by immunofluorescence staining. Data was from three independent experiments and one representative result is shown here. (D) The effect of Au₂₅Sv₉ on the bone resorption activity of formed osteoclasts *in vitro* was assessed by a pit formation assay on surface of osteoassay plate. Data was from three independent experiments and one representative result is shown here. (E) Quantitative analysis of the ratio of resorption pits in unit area of the osteoassay plate. The data is presented as mean ± Standard deviation of triplicate experiments, *P < 0.05, **P < 0.01, compared to the RANKL only group.

Au₂₅Sv₉ significantly inhibit inflammatory bone destruction in CIA mice

Since gold cluster can inhibit osteoclast differentiation and inflammation *in vitro*, we examined its effect on preventing inflammation-induced bone loss *in vivo*. Collagen induced arthritis (CIA) in mice was used as a model to evaluate the therapeutic effect of Au₂₅Sv₉ [5]. According to the acute toxicity test (LD50 = 97.18 mg Au/kg body weight), the therapeutic regimen of Au₂₅Sv₉ in CIA mice was determined to

intraperitoneal injection (i.p.) of 5 mg Au/kg body weight per day. Changes in body weight of each group were monitored throughout the course of treatment. The data showed that CIA model can reduce the gain of body weight, but Au₂₅Sv₉ treatment can significantly reverse this reduction, especially in the fourth and fifth weeks (Figure 5A). The paws of CIA mice were found to have erythema swelling at week 4 after the first injection of collagen compared to saline-injected mice. The extent of arthritis reached its

maximum at week 5-6. Treatment with Au₂₅Sv₉ (5 mg Au/kg) significantly suppressed the severity of clinical arthritis ($p < 0.05$), whereas no obvious suppressive effect was observed in vehicle-treated CIA mice, such as by paw swelling and arthritis clinical score (Figure 5B-C). Articular bone destruction was performed by microCT (μ CT) scan plus histological analysis on the ends of metatarsal, to determine whether treatment with Au₂₅Sv₉ was effective in reducing severe bone destruction. The microCT observations revealed that CIA caused very severe bone erosion and formed obvious absorption holes at the ends of metatarsal, while Au₂₅Sv₉ treatment can effectively attenuate this destruction (Figure 5D). Histological observations within joints were consistent with microCT scan results, indicating that CIA caused severe damage in both cartilage and bone, while Au₂₅Sv₉ treatment effectively attenuates the erosion (Figure 5E). Haematoxylin and eosin sections were scored according to histopathological changes, and analysis showed Au₂₅Sv₉ significantly prevented CIA induced cartilage and bone damage (Figure 5F). Moreover, no inflammation or tissue destruction was observed in HE sections from normal

mice, but untreated CIA mice revealed prominent destructive inflammation of periarticular tissues and synovial hyperplasia (Figure 5E). In contrast, such inflammatory cellular infiltration and synovial hyperplasia were markedly reduced in mice treated with 5 mg Au/kg Au₂₅Sv₉ (Figure 5F). These results suggested the gold cluster can effectively attenuate inflammation and inflammatory bone destruction synergistically in chronic inflammatory diseases.

The systematic toxicity of gold cluster was determined in mice treated with 5 mg Au/kg Au₂₅Sv₉ for 28 days, except for the acute toxicity of gold cluster (LD₅₀ = 97.18 mg Au/kg body weight). Both blood routine and blood biochemistry examinations of Au₂₅Sv₉ treated mice showed the same pattern as normal mice, indicating that Au₂₅Sv₉ injection did not induce significant hematological toxicity (Table S1 and Table S2). The histomorphology changes of main organs were also observed to determine whether the Au₂₅Sv₉ treatment induced organ damage. The observation indicated that Au₂₅Sv₉ injection did not induce any obvious damage to the detected organs (Figure S2). These results indicated that Au₂₅Sv₉ can reduce the major side-effects of traditional gold drugs.

Au₂₅Sv₉ suppresses pro-inflammation cytokines and inflammation-induced RANKL expression *in vivo*

To elucidate the *in vivo* therapeutic mechanism of Au₂₅Sv₉ in inflammation-induced bone loss, the effect of Au₂₅Sv₉ on biochemical parameters was detected in CIA mice. After treatment of Au₂₅Sv₉ in CIA mice, articular cytokines levels of TNF- α , IL-1 β and IL-6 were measured by ELISA to elucidate the mechanism of inflammation inhibition in arthritic. The levels of TNF- α , IL-1 β and IL-6 in the hind paws of CIA mice were significantly increased on day 28 post-immunization compared to baseline levels of normal mice (Figure 6A-C). Treatment with Au₂₅Sv₉ resulted in a significant reduction in these cytokines compared to the high levels found in vehicle treated CIA mice (Figure 6A-C). High level of RANKL in CIA mice is a key factor in osteoclastogenesis and is crucial for bone destruction under chronic inflammation [4, 5]. The inflammatory cytokines detected in this study can stimulate RANKL production by lymphocytes and fibroblasts [26, 27]. Therefore, RANKL expression in the hind paw of CIA mice was detected by immunoblotting after Au₂₅Sv₉ treatment or vehicle treatment. The results indicated that collagen immunization increased the

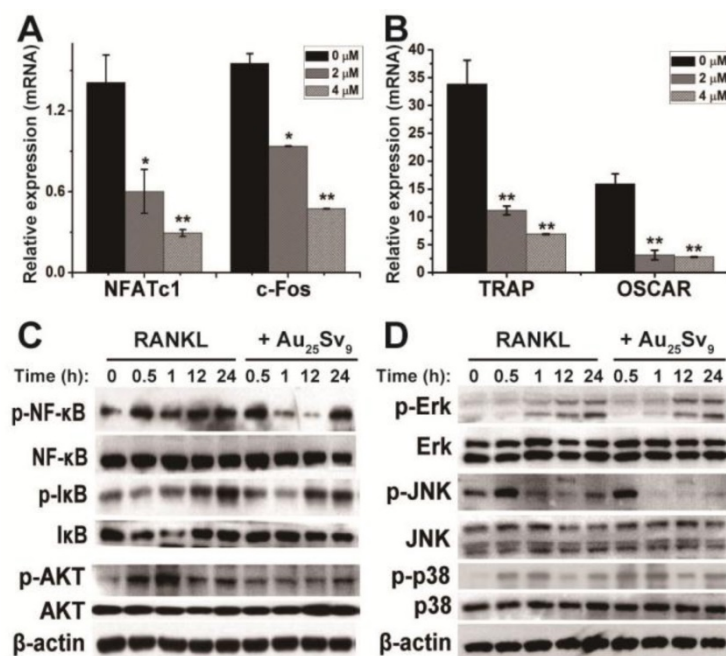


Figure 4. Effects of Au₂₅Sv₉ on the expression of osteoclastogenic genes and RANKL-induced signaling pathways. (A) RAW264.7 cells were induced with RANKL in the presence or absence of Au₂₅Sv₉, and the expression of NFATc1 and c-Fos was analyzed by real-time RT-PCR at 48 h, GAPDH was used as the loading control. The data is presented as mean \pm Standard deviation of triplicate experiments, * $P < 0.05$, ** $P < 0.01$, compared to the RANKL only group. (B) The expression of TRAP and OSCAR was analyzed by real-time RT-PCR at 48 h. The data is presented as mean \pm Standard deviation of triplicate experiments, * $P < 0.05$, ** $P < 0.01$, compared to the RANKL only group. (C) Western blotting for total NF- κ B, I κ B, AKT and their phosphorylated form was performed at indicated time. (D) Phosphorylation of MAPKs (ERK, p38 and JNK) was also assessed by western blotting. β -actin was used as the loading control. Data was from three independent experiments and one representative result is shown here.

expression of RANKL in joint, and supplementation with Au₂₅Sv₉ was effective in inhibiting this overexpression compared to vehicle treatment (Figure 6D). Au₂₅Sv₉ can effectively inhibit RANKL-induced osteoclastogenesis *in vitro* by suppressing the activation of NF-κB pathway. Therefore, phosphorylation of NF-κB in the joints of CIA mice was detected by immunohistochemical staining in histologic sections. The results revealed that the levels of phosphorylated NF-κB (p-NF-κB) were increased in CIA mice compared to normal mice, whereas Au₂₅Sv₉ treatment significantly inhibited this activation (Figure 6E). These data indicated that the gold cluster can suppress the production of pro-inflammatory cytokines, and that related RANKL expression can improve bone destruction in CIA joints by inhibiting the activation of NF-κB pathway *in vivo*.

Discussion

A large number of patients continue to suffer from severe bone destruction caused by chronic

inflammation and the resultant dysfunction [1, 28]. However, anti-resorptive therapies alone does not prevent focal bone loss in clinical trials, suggesting that chronic inflammation promotes an overall catabolic state with increased osteoclast differentiation and resorptive activity [28]. Pro-inflammatory cytokines produced by macrophages are crucial in initiating the associated bone destruction in chronic inflammatory diseases, such as TNF-α and IL-1β [18]. These cytokines can promote the differentiation and activation of bone-resorbing osteoclasts through increasing the expression of RANKL [7, 19]. Under RANKL stimulation, osteoclasts can be differentiated from monocyte/macrophage lineage precursor. In this study, LPS-induced over-production of pro-inflammatory cytokines and RANKL-induced osteoclastogenesis as well as bone resorption *in vitro* were all significantly inhibited by Au₂₅Sv₉ in a dose-dependent manner. RANKL stimulation will trigger a variety of intracellular signal transduction events leading to up-regulation of osteoclast-specific genes [7]. A crucial target downstream of RANKL signaling is the activation of NF-κB, which plays a key role in osteoclast differentiation [6]. The central role for NF-κB in osteoclastogenesis has been demonstrated by gene-specific deletion of the NF-κB subunits that caused severe osteopetrosis due to the absence of osteoclasts [29, 30]. And a peptide named NBD that selectively blocking the activation of NF-κB was reported to inhibit the RANKL-induced osteoclast differentiation effectively both *in vitro* and *in vivo* [31]. Therefore, the RANKL-induced osteoclast differentiation might be prevented by blocking NF-κB in osteoclast precursors. Previous studies reported, the gold nanoparticles prepared by electrical explosion or β-cyclodextrin (CD) conjugated could inhibit RANKL-induced osteoclast differentiation *in vitro* were also involved in the disturbing of NF-κB activation

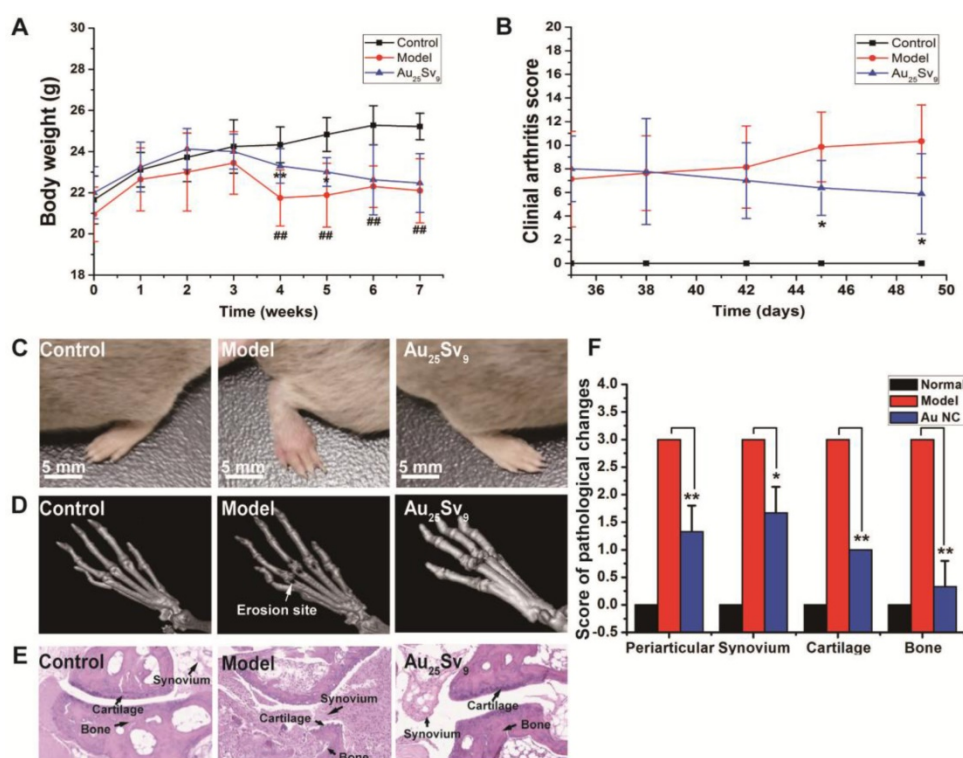


Figure 5. Effects of Au₂₅Sv₉ on bone destruction in CIA inflammation mice. (A) Change of body weight in each group was measured every week. The data is presented as mean ± Standard deviation, n = 10 per group, *P < 0.05, **P < 0.01, compared to the CIA model group, ### P < 0.01, compared to the normal control group. (B) According to the extent of erythema and swelling, the clinical arthritis score was assessed by grading each paw from 0 to 4, and a mean score was given for each mouse. The data is presented as mean ± Standard deviation, n = 10 per group, *P < 0.05, compared to the CIA model group. (C) Representative photographs of CIA mice treated with vehicle or Au₂₅Sv₉, and non-immunized normal mouse was used as control group, n = 10 per group. (D) Representative photographs of μCT observation in each group of CIA mice treated with vehicle or Au₂₅Sv₉, and normal control group, n = 5 per group. The typical site of severe bone erosion is marked by white arrows in Model group. (E) Representative histopathological images of joint sections from each group of CIA mice treated with vehicle or Au₂₅Sv₉, and normal mice, n = 5 per group. The cartilage, bone and synovium were indicated by black arrows respectively in each image. (F) Histological scores of cartilage and bone erosion as well as inflammation index in CIA mice treated with vehicle or Au₂₅Sv₉ (Au NC), and normal mice. The data is presented as mean ± Standard deviation, n = 5 per group, *P < 0.05, **P < 0.01, compared to the CIA model group.

[32, 33]. Thus, the effect of Au₂₅Sv₉ on RANKL-induced NF-κB activation was clarified in this study. Au₂₅Sv₉ indeed inhibited RANKL-induced NF-κB activation and up-regulation of osteoclast-specific genes effectively (Figure 4). Considering the activated NF-κB is also responsible for the overexpression of pro-inflammatory genes in macrophages in chronic inflammatory diseases [19, 20]. Inhibiting the activation of NF-κB in monocyte-macrophages might offer an effective therapeutic approach for preventing inflammatory bone destruction. Indeed, the NBD peptide not only avoided bone destruction in inflammatory joints of arthritis mice but also suppressed the pro-inflammatory cytokine production almost completely [31]. However, because NF-κB has other crucial roles in vary cells, such as anti-apoptotic activity, it has been suggested that its overall suppression may be limited use due to the possibility of extensive apoptosis [31]. This concept was supported by a report that conditional deletion of IKKβ to complete block NF-κB may induce enhanced apoptosis and damage [34]. Hence, inhibition of abnormal activated NF-κB in monocyte-macrophages relatively specific may be beneficial in preventing inflammatory bone destruction without affecting other physiological functions. In the course of chrysotherapy, gold was found to concentrate within inflamed synovial tissues selectively, and forming gold-rich deposits in synovial macrophages in

rheumatoid patients [35-37]. Thus, macrophages have been assumed to be the target of gold reagents, which giving the gold cluster a certain targeting ability. In addition, the strong positive charge of the Sv peptide could assist the gold cluster to penetrate the cell membrane, which has been demonstrated in our previous study [13]. We deduce the Au₂₅Sv₉ clusters possess an adequacy targeting ability to macrophages which would facilitate their therapeutic effects in inflammatory bone destruction. In addition, RANKL has been identified to support the survival of mature osteoclasts involved in the activation of AKT [6]. The results revealed Au₂₅Sv₉ also attenuated the RANKL-induced phosphorylation of AKT.

Although several gold nanoparticles were reported to suppress inflammation or prevent RANKL-induced osteoclast differentiation *in vitro* respectively, their activity in preventing inflammatory bone destruction *in vivo* has not been determined [32, 33, 38]. The Au₂₅Sv₉ clusters significantly inhibit LPS-induced and RANKL-induced activation of NF-κB in macrophages to suppress the overexpression of pro-inflammatory factors and osteoclastogenesis simultaneously. We therefore suggest the gold cluster might emerge unparalleled advantages in the prevention of inflammatory bone destruction by combining these two activities. Collagen-induced arthritis (CIA) mice, which develop a polyarthritis with severe cartilage and bone destruction, were used

to evaluate the therapeutic effects of Au₂₅Sv₉ on inflammation-induced bone destruction *in vivo*. Collagen immunization increased the levels of several proinflammatory cytokines in CIA joints, while the supplementation of Au₂₅Sv₉ effectively reduced their levels, including TNF-α, IL-1β and IL-6. The subsequent up-regulation of RANKL in joint was also suppressed by Au₂₅Sv₉. Therefore, a schematic diagram was proposed to describe the action model of Au₂₅Sv₉ in preventing inflammation related bone destruction (Figure 7). Au₂₅Sv₉ suppresses the expression of pro-inflammatory factors in macrophages to inhibit over-expression of RANKL within inflammatory sites, thereby indirectly reducing osteoclastogenesis and subsequent bone erosion. On the other hand, Au₂₅Sv₉ blocks signal transduction from RANKL stimulation to certain transcription factors to inhibit differentiation and activation of osteoclasts directly (Figure 7). It is

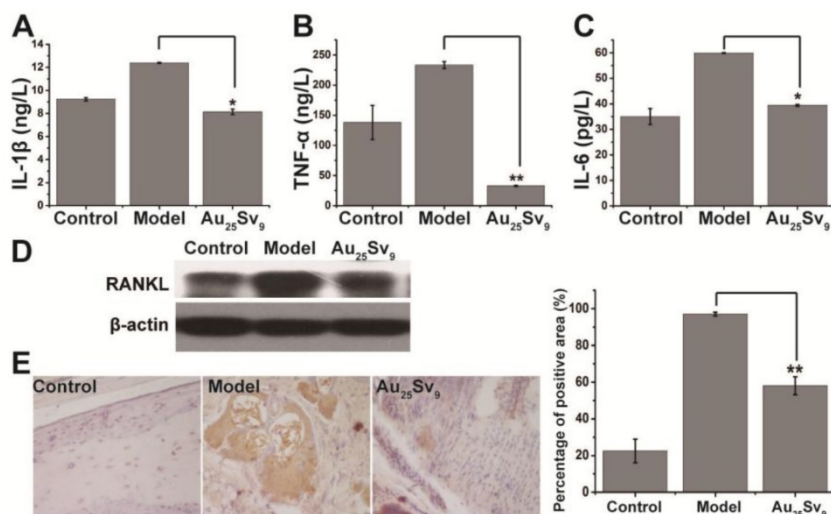


Figure 6. Effects of Au₂₅Sv₉ on the expression of pro-inflammation cytokines and RANKL *in vivo*. (A-C) The levels of pro-inflammatory cytokines (TNF-α, IL-1β, and IL-6) in the articular tissue of CIA mice, treated with vehicle or Au₂₅Sv₉ and normal control group. The data is presented as mean ± Standard deviation, n = 5 per group, *P < 0.05, **P < 0.01, compared to the CIA model group. (D) The expression of RANKL in the articular tissue of CIA mice treated with vehicle or Au₂₅Sv₉, and normal control group, were detected by Western blotting. β-actin was used as the loading control. Data was from three independent mice of each group and one representative result is shown here. (E) Immunohistochemistry was performed for p-NF-κB antibody to detect the activation of NF-κB in the articular tissue of CIA mice treated with vehicle or Au₂₅Sv₉, and normal control group, n = 5 per group and representative photographs were presented. The level of phosphorylated NF-κB in each group was quantized and compared. **P < 0.01, compared to the CIA model group.

also worth noting that no obvious side-effect on test mice was observed in this study, particularly with regard to hematological toxicity and damage to main organs, which will facilitate the clinical application of gold cluster in the future.

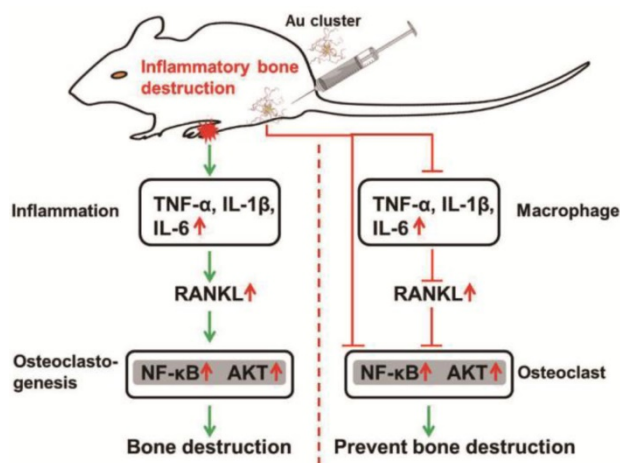


Figure 7. Biological mechanisms that involving in the prevention of inflammatory bone destruction *in vivo* of Au₂₅S₁₉ gold cluster.

Conclusion

In this study, we prepared a novel gold cluster to ameliorate inflammation associated bone destruction *in vivo*. We demonstrate that the gold cluster strongly suppresses RANKL-mediated osteoclast formation *in vitro* which related to the inhibition of NF-κB pathway activation. In addition, this cluster significantly reduced the destruction of bone and cartilage in mice by reducing the levels of pro-inflammatory cytokines (TNF-α, IL-1β and IL-6) and they triggered RANKL. To our knowledge, this study is the first to demonstrate the therapeutic effect of gold clusters on inflammation-induced bone destruction.

Acknowledgements

This work was supported by the National Natural Science Foundation of China (21425522, 21727817, 11621505 and 31700874), Beijing Science and Technology Commission Special Project for Frontier Technology in Life Sciences (Z171100000417008) and Beijing municipal high level innovative team building program (IDHT20180504).

Author contributions

Q.Y., X.G. and F.G. designed the study. Q.Y., Y.Y., P.C., X. Z., J. Y., and K. H. conducted the experiments. Q.Y., F.G., P.C., L. G. and X. R. analyzed the data. Q.Y. and X.G. wrote the manuscript. All authors discussed the results and critically revised the manuscript.

Supplementary Material

Supplementary figures and tables.

<http://www.thno.org/v09p1825s1.pdf>

Competing Interests

The authors have declared that no competing interest exists.

References

- Smolen JS, Aletaha D, McInnes IB. Rheumatoid arthritis. *Lancet*. 2016; 388: 2023-38.
- Scott DL, Pugner K, Kaarela K, Doyle DV, Woolf A, Holmes J, et al. The links between joint damage and disability in rheumatoid arthritis. *Rheumatology*. 2000; 39: 122-32.
- Jimi E, Aoki K, Saito H, D'Acquisto F, May MJ, Nakamura I, et al. Selective inhibition of NF-kappa B blocks osteoclastogenesis and prevents inflammatory bone destruction *in vivo*. *Nat Med*. 2004; 10: 617-24.
- Findlay DM, Haynes DR. Mechanisms of bone loss in rheumatoid arthritis. *Modern Rheumatology*. 2005; 15: 232-40.
- Cantley MD, Smith MD, Haynes DR. Pathogenic bone loss in rheumatoid arthritis: Mechanisms and therapeutic approaches. *International Journal of Clinical Rheumatology*. 2009; 4: 561-82.
- Kikuta J, Ishii M. Osteoclast migration, differentiation and function: novel therapeutic targets for rheumatic diseases. *Rheumatology*. 2013; 52: 226-34.
- Boyle WJ, Simonet WS, Lacey DL. Osteoclast differentiation and activation. *Nature*. 2003; 423: 337-42.
- Schett G. Cells of the synovium in rheumatoid arthritis - Osteoclasts. *Arthritis Res Ther*. 2007; 9: 203-8.
- Romas E, Gillespie MT, Martin TJ. Involvement of receptor activator of NFkappaB ligand and tumor necrosis factor-alpha in bone destruction in rheumatoid arthritis. *Bone*. 2002; 30: 340-6.
- Yuan Q, Wang YL, Zhao LN, Liu R, Gao FP, Gao L, et al. Peptide protected gold clusters: chemical synthesis and biomedical applications. *Nanoscale*. 2016; 8: 12095-104.
- Luo ZT, Zheng KY, Xie JP. Engineering ultrasmall water-soluble gold and silver nanoclusters for biomedical applications. *Chem Commun*. 2014; 50: 5143-55.
- Shu J, Qiu G, Mohammad I. A Semi-automatic Image Analysis Tool for Biomarker Detection in Immunohistochemistry Analysis. 2013: 937-42.
- Liu R, Wang YL, Yuan Q, An DY, Li JY, Gao XY. The Au clusters induce tumor cell apoptosis via specifically targeting thioredoxin reductase 1 (TrxR1) and suppressing its activity. *Chem Commun*. 2014; 50: 10687-90.
- Li Q, Yuan Q, Zhao M, Yao YW, Gao L, Liu R, et al. Au nanoclusters suppress chronic lymphocytic leukaemia cells by inhibiting thioredoxin reductase 1 to induce intracellular oxidative stress and apoptosis. *Sci Bull*. 2017; 62: 537-45.
- Wu ZW, Gayathri C, Gil RR, Jin RC. Probing the Structure and Charge State of Glutathione-Capped Au-25(SG) Clusters by NMR and Mass Spectrometry. *J Am Chem Soc*. 2009; 131: 6535-42.
- Zhu M, Lanni E, Garg N, Bier ME, Jin R. Kinetically controlled, high-yield synthesis of Au-25 clusters. *J Am Chem Soc*. 2008; 130: 1138-9.
- Lam J, Abu-Amer Y, Nelson CA, Fremont DH, Ross FP, Teitelbaum SL. Tumour necrosis factor superfamily cytokines and the pathogenesis of inflammatory osteolysis. *Ann Rheum Dis*. 2002; 61 Suppl 2: ii82-3.
- Feldmann M, Brennan FM, Foxwell BM, Maini RN. The role of TNF alpha and IL-1 in rheumatoid arthritis. *Current directions in autoimmunity*. 2001; 3: 188-99.
- Bondeson J. The mechanisms of action of disease-modifying antirheumatic drugs: A review with emphasis on macrophage signal transduction and the induction of proinflammatory cytokines. *Gen Pharmacol*. 1997; 29: 127-50.
- Tas SW, Remans PHJ, Reedquist KA, Tak PP. Signal transduction pathways and transcription factors as therapeutic targets in inflammatory disease: Towards innovative antirheumatic therapy. *Curr Pharm Design*. 2005; 11: 581-611.
- Nakashima T, Wada T, Penninger JM. RANKL and RANK as novel therapeutic targets for arthritis. *Curr Opin Rheumatol*. 2003; 15: 280-7.
- Naidu VG, Dinesh Babu KR, Thwin MM, Satish RL, Kumar PV, Gopalakrishnakone P. RANKL targeted peptides inhibit osteoclastogenesis and attenuate adjuvant induced arthritis by inhibiting NF-kappaB activation and down regulating inflammatory cytokines. *Chemico-biological interactions*. 2013; 203: 467-79.
- Dankbar B, Fennen M, Brunert D, Hayer S, Frank S, Wehmeyer C, et al. Myostatin is a direct regulator of osteoclast differentiation and its inhibition reduces inflammatory joint destruction in mice. *Nature medicine*. 2015; 21: 1085-90.
- Geng H, Chang YN, Bai X, Liu ST, Yuan Q, Gu WH, et al. Fullerol nanoparticles suppress RANKL-induced osteoclastogenesis by inhibiting differentiation and maturation. *Nanoscale*. 2017; 9: 12516-23.

25. Takito J, Otsuka H, Yanagisawa N, Arai H, Shiga M, Inoue M, et al. Regulation of Osteoclast Multinucleation by the Actin Cytoskeleton Signaling Network. *J Cell Physiol.* 2015; 230: 395-405.
26. Wong PKK, Quinn JMW, Sims NA, van Nieuwenhuijze A, Campbell IK, Wicks IP. Interleukin-6 modulates production of T lymphocyte-derived cytokines in antigen-induced arthritis and drives inflammation-induced osteoclastogenesis. *Arthritis Rheum.* 2006; 54: 158-68.
27. Mihara M, Moriya Y, Kishimoto T, Ohsugi Y. Interleukin-6 (IL-6) Induces the Proliferation of Synovial Fibroblastic Cells in the Presence of Soluble IL-6 Receptor. *Brit J Rheumatol.* 1995; 34: 321-5.
28. Rehman Q, Lane NE. Bone loss - Therapeutic approaches for preventing bone loss in inflammatory arthritis. *Arthritis Res.* 2001; 3: 221-7.
29. Iotsova V, Caamano J, Loy J, Yang Y, Lewin A, Bravo R. Osteopetrosis in mice lacking NF-kappa B1 and NF-kappa B2. *Nature medicine.* 1997; 3: 1285-9.
30. Franzoso G, Carlson L, Xing LP, Poljak L, Shores EW, Brown KD, et al. Requirement for NF-kappa B in osteoclast and B-cell development. *Gene Dev.* 1997; 11: 3482-96.
31. Jimi E, Aoki K, Saito H, D'Acquisto F, May MJ, Nakamura I, et al. Selective inhibition of NF-kappa B blocks osteoclastogenesis and prevents inflammatory bone destruction in vivo. *Nature medicine.* 2004; 10: 617-24.
32. Heo DN, Ko WK, Moon HJ, Kim HJ, Lee SJ, Lee JB, et al. Inhibition of Osteoclast Differentiation by Gold Nanoparticles Functionalized with Cyclodextrin Curcumin Complexes. *Acs Nano.* 2014; 8: 12049-62.
33. Sul OJ, Kim JC, Kyung TW, Kim HJ, Kim YY, Kim SH, et al. Gold nanoparticles inhibited the receptor activator of nuclear factor-kappaB ligand (RANKL)-induced osteoclast formation by acting as an antioxidant. *Bioscience, biotechnology, and biochemistry.* 2010; 74: 2209-13.
34. Chen LW, Egan L, Li ZW, Greten FR, Kagnoff MF, Karin M. The two faces of IKK and NF-kappaB inhibition: prevention of systemic inflammation but increased local injury following intestinal ischemia-reperfusion. *Nature medicine.* 2003; 9: 575-81.
35. Vernonroberts B, Dore JL, Jessop JD, Henderson WJ. Selective Concentration and Localization of Gold in Macrophages of Synovial and Other Tissues during and after Chrysotherapy in Rheumatoid Patients. *Ann Rheum Dis.* 1976; 35: 477-86.
36. Nakamura H, Igarashi M. Localization of Gold in Synovial-Membrane of Rheumatoid-Arthritis Treated with Sodium Aurothiomalate - Studies by Electron-Microscope and Electron-Probe X-Ray Microanalysis. *Ann Rheum Dis.* 1977; 36: 209-15.
37. Darien BJ, Sims PA, Kruseelliott KT, Homan TS, Cashwell RJ, Cooley AJ, et al. Use of Colloidal Gold and Neutron-Activation in Correlative Microscopic Labeling and Label Quantitation. *Scanning Microscopy.* 1995; 9: 773-80.
38. Brown CL, Whitehouse MW, Tiekink ER, Bushell GR. Colloidal metallic gold is not bio-inert. *Inflammopharmacology.* 2008; 16: 133-7.